Experimental determination of line-intensity ratios of transitions within the $n=2$ complex of Be I–like ions (Cl XIV to Cr XXI)

L. K. Huang, S. Lippmann, T. L. Yu, B. C. Stratton,* and H. W. Moos
Department of Physics and Astronomy, The Johns Hopkins University, Baltimore, Maryland 21218

M. Finkenthal
Racah Institute of Physics, Hebrew University, Jerusalem, Israel

W. L. Hodge, W. L. Rowan, B. Richards, and P. E. Phillips
Fusion Research Center, The University of Texas, Austin, Texas 78712

A. K. Bhatia
Goddard Space Flight Center, Greenbelt, Maryland 20771
(Received 3 November 1986)

The $n=2$ to $n=2$ transition lines in the Be I ion sequence of moderately-high-Z elements (Cl to Cr) were studied in the emission spectra of the Texas Experimental tokamak plasma when the appropriate elements were injected. A number of lines were identified for the first time. The relative brightnesses of the spectral lines were measured by an instrument with a photoelectric detector which was photometrically calibrated against synchrotron radiation. The brightness ratios of the $2s2p\,^3P_2-2p^2\,^3P_2$ (R) and the $2s^2\,^1S_0-2s2p\,^3P_1$ (R^*) transitions to the resonance $2s^2\,^1S_0-2s2p\,^1P_1$ line were determined and compared with theoretical predictions. For R, the ratio of the experimental to the theoretical values was 1.01 ± 0.19 and for R^*, 0.84 ± 0.17, indicating a good agreement with the calculations of relative level populations using collision strengths computed by the distorted-wave approximation.

I. INTRODUCTION

The atomic transitions within the $n=2$ complex of ions of moderately-high-Z elements ($Z>17$) isoelectronic with Be I emit in the extreme-ultraviolet (euv) spectral region. These lines may be observed in spectra of both high-temperature ($T_e\approx1$ keV) laboratory and astrophysical plasmas. The $2s^2\,^1S_0-2s2p\,^1P_1$ and $2s2p\,^3P-2p^2\,^3P$ transitions have been identified mainly in high-density laser-produced plasmas[1,2] while the $2s^2\,^1S_0-2s2p\,^3P_1$ transitions of some of the elements under consideration have been measured in solar flare spectra.[3,4] A few line identifications within this sequence have been reported from work done on tokamak plasmas.[5–8] A critical survey on the status of line identifications in the Be I isoelectronic sequence can be found in a recent paper by Edlén.[9]

The usefulness of various line ratios of Be I–like ions for plasma diagnostics has been discussed in a number of papers.[10–15] In these papers, level populations have been calculated in order to derive electron densities and electron temperatures of astrophysical—particularly, solar—plasmas or laser-produced plasmas from measured line ratios. These lines are also potentially useful as diagnostics for the magnetically confined plasmas used in controlled thermonuclear research. Such applications include deriving the electron temperature or density from measured line-intensity ratios in cases in which a more direct diagnostic technique is not available, determining the radiated power losses and the impurity densities from measured line brightnesses, and studying the impurity transport by using the time history and spatial distribution of the emissions.

However, it was not known whether the theoretical calculations mentioned above could be used with confidence. An example of a long-standing problem in the use of these line ratios as electron density diagnosis is the difficulty in interpreting the Ca XVII emissions in solar flare spectra.[4,10,11] The measured line ratio $I(\lambda=193\ \text{Å})/I(\lambda=233\ \text{Å})$ of Ca XVII for the August 9, 1973 flare was 50. (The brightness unit, photons/sr cm^2 sec, is used throughout this paper.) For this ratio, the computed line ratios of Bhatia *et al.*[10] and Dufton *et al.*[11] imply that the electron density of the August 9, 1973 solar flare was greater than 5×10^2 cm^{-3}. But line ratios of other ions, for instance, $I(\lambda=225\ \text{Å})/I(\lambda=209\ \text{Å})$ of Ca XVI, $I(\lambda=257\ \text{Å})/I(\lambda=244\ \text{Å})$ of Ar XIV, and $I(\lambda=182\ \text{Å})/I(\lambda=201\ \text{Å})$ of Ca XV (Ref. 4), lead to a density less than 5×10^{11} cm^{-3} in the same solar flare. For an electron density less than 5×10^{11} cm^{-3}, the above-referenced calculations predicted the line ratio $I(\lambda=193\ \text{Å})/I(\lambda=233\ \text{Å})$ of Ca XVII to be greater than 150. The cause of the discrepancy may have been experimental, caused by unsuspected spectral blends and errors in the photometric calibration, or it could have been theoretical, caused by inaccuracies in the calculations of the line ratios. It is clear that carefully controlled experiments in a laboratory plasma such as in a tokamak in which the electron densities are measured by nonspectroscopic means would remove much of the uncertainty in the use of these line ratios.

Stratton *et al.*[16] measured line ratios in the Princeton Large Torus tokamak plasma for a number of transitions in the B I to C I isoelectronic sequences for Ti, Cr, Ni, and Ge. Generally, they found good agreement between the measured and the computed values for which the distorted-wave approximation was used to compute electron collision strengths. However, no checks have been made at somewhat lower Z where this type of computations may be less reliable or, in particular, for the Be I sequence. (A study of C III, O V, F VI, and Ne VII by Finkenthal *et al.*[17] has shown that computations for the Be I sequence based on the distorted-wave approximation are not adequate at very low Z.) Thus the study reported here extends the investigation to this domain.

The importance of experimental determinations of these lines is based not only on the needs of plasma diagnostics but also on the fact that it can improve the understanding of the electron-ion collision processes. The most extensive line-ratio computation so far has been done for Ar to Kr using collision strengths computed by the distorted-wave approximation.[18] Calculations based on the R-matrix method are available for a smaller number of these elements.[11,19] For the low-Z Be I–like ions, recent experimental results[17] agree better with computations based on the R-matrix method than on those using the distorted-wave function approximation. But as discussed in Sec. III, the distorted-wave approximation is expected to be more accurate with increasing Z. However, as there are as yet no precise theoretical criteria with which to judge the precision of the theories, this does not guarantee that the computed line ratios actually will agree with the experimental values. Thus it is important to measure some of the line ratios of the stronger lines in a systematic way along the isoelectronic sequence, in particular, for the moderately-high-Z elements in order to explore the atomic collision processes experimentally.

The experiment described here recorded a large number of spectra for Cl to Cr emitted from the Texas Experimental (TEXT) tokamak plasmas. This paper reports the measurements of newly observed $2s^2\,{}^1S_0-2s2p\,{}^3P_1$ transition lines of Be I–like ions, Ar XV to Cr XXI, and a thorough comparison with theoretical predictions of two measured line ratios,

$$R = I(2s\,2p\,{}^3P_2-2p^2\,{}^3P_2)/I(2s^2\,{}^1S_0-2s\,2p\,{}^1P_1) \quad (1)$$

and

$$R^* = I(2s^2\,{}^1S_0-2s\,2p\,{}^3P_1)/I(2s^2\,{}^1S_0-2s\,2p\,{}^1P_1)\ . \quad (2)$$

[For a simplified diagram of the energy level structure, see Fig. 8(c) in Sec. III.] The data were obtained from plasmas in which the electron temperature and density were known and well controlled. In addition, it was possible to vary the electron densities over a factor of 5, making possible a more thorough comparison between the experiment and theory. Generally good agreement was found between the measured values and the predictions, leading to confidence both in the theoretical approach and in the line ratios as diagnostic tools for the determination of electron densities in both laboratory and astrophysical plasmas.

II. EXPERIMENTAL DETAILS

The TEXT tokamak[20] plasma toroidal radius was 100 cm, and its minor radius was 27 cm. A typical discharge lasted 500 ms. The experiment was conducted at three line average electron densities, 1.6×10^{13}, 3.5×10^{13}, and 8.0×10^{13} cm^{-3}. Electron-density distribution profiles along the minor radius were determined by the far-infrared interferometer (FIR). The electron temperature, which was measured by Thomson scattering of ruby laser light, at the tokamak center was about 1 keV. Typical profiles of the electron density and temperature are shown in Fig. 1.

The elements to be studied were injected by the laser blow-off from thin films.[21] The amount of injected elements was adjusted to give a maximal enhancement of the measured lines while maintaining stable and reproducible discharges.

The grazing-incidence (2°) time-resolving spectrograph[22] (GRITS) used in this experiment has a holographic grating of 1200 g/cm, an entrance slit of 50 μm$\times$1.0 cm, and an image intensifier detector mounted on a 1-m Rowland circle. A MgF_2 photocathode is deposited on a microchannel plate which is coupled, via a phosphor screen and fiber optics, to a 1024-pixel photodiode array. Both the photometric and geometric properties of the detector are quite stable which considerably improved the reliability of the data analysis. The spectral resolution is 0.7 Å. The detector is set at preselected positions along the Rowland circle over the 15–360-Å range. The bandwidth for simultaneous coverage ranges from 40 to 80 Å, depending upon the detector position. The photodiode array integrates incoming signals for a period of 5.4 ms and is continuously scanned 32 times during every tokamak discharge. Each scan records a complete spectrum (called a frame).

The spectrometer was mounted on the top of the

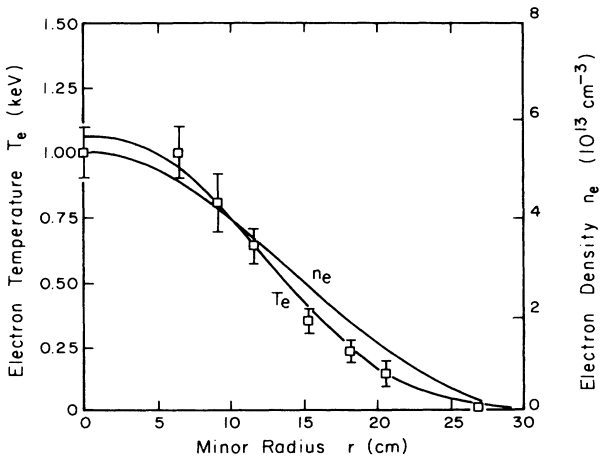

FIG. 1. Typical electron-density and temperature profiles in a TEXT tokamak plasma discharge as a function of distance from the discharge center along the minor radius. The density was obtained by the FIR interferometer. The average of the electron density across the plasma is about 3.0×10^{13} cm^{-3}. The temperature is measured by Thomson scattering.

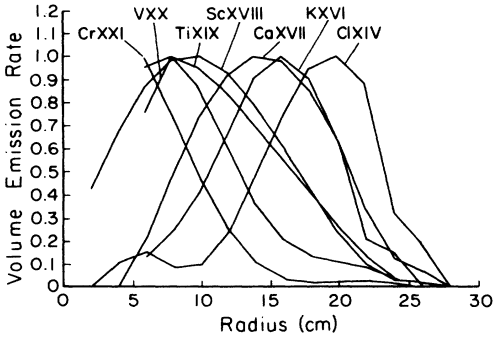

FIG. 2. Relative volume-emission profiles of the $2s^2\,{}^1S_0$–$2s2p\,{}^1P_1$ transitions of the Be I–like ions. Peaks occurred near the point where the electron temperature was equal to the ionization equilibrium temperature. With increasing Z, the peaks move closer to the center.

tokamak. A drive mechanism was provided which allowed the view of different chords of the plasma in a shot-by-shot radial scan. The spatial resolution along the plasma minor radius was 2 cm. The radial profiles of the impurity emission were obtained by Abel inverting[23] the chord brightnesses. Figure 2 shows the measured volume emission profiles of the $2s^2\,{}^1S_0$–$2s2p\,{}^1P_1$ transitions for Be I ions of different elements.

The values of the electron density and temperature of the plasma for a given Be I–like ions were determined by comparing the radial emission profiles with the electron-density and the electron-temperature profiles. Within the accuracy of the electron-temperature measurement, each studied ion population reached a maximum concentration at a radial position with electrons at the ionization-equilibrium temperature,[24,25] which is close to the half ionization potential.[26] Table I shows both electron density and temperature in the plasma where the peak emissions were found during discharges at an average line electron density of 3.5×10^{13} cm^{-3}.

The wavelength calibration was based on well-known lines of carbon, oxygen, titanium, and iron ions, emitted from the TEXT plasma. A polynomial fitting procedure interpolated the wavelength readings between the known lines. The uncertainty in determining an unknown line wavelength is 0.2 Å.

The techniques used to identify lines emitted by injected elements in a tokamak plasma have been described in detail elsewhere.[27,28] In order to remove the intrinsic element emission background, a spectrum taken before the injection was always subtracted from that taken after the injection. Figure 3 shows how a Ti XIX line at 328.34 Å was separated from an intrinsic element line of Cr XIII 328.29 Å by the subtraction. Due to differences in the ionization rates, differences in the inward transport rate, and the unequal confinement times, time history plots of each line could be used to indicate the ionization state of each line of the injected element, as shown in Fig. 4. The spatial profile of the line emission was also an important signature of a specific species (Fig. 2) because of the different spatial locations of ions in the tokamak.

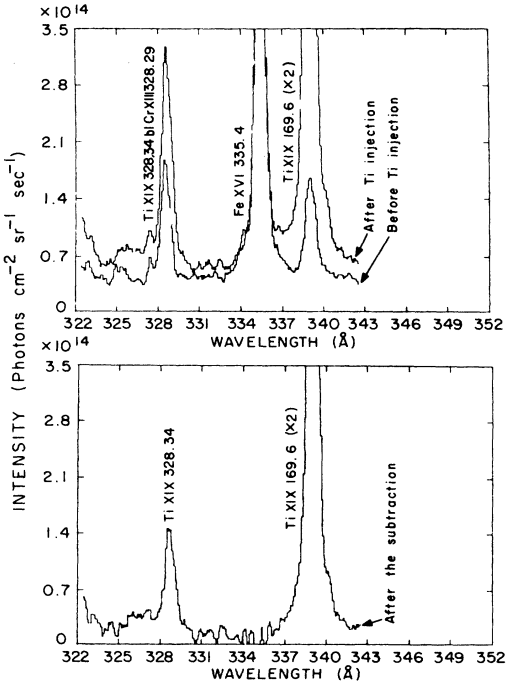

FIG. 3. Subtraction of a spectrum before the injection of titanium from a spectrum after the injection. The Ti XIX 328.34-Å line is blended with the Cr XIX 328.29-Å line. The signal due to the intrinsic Cr XIII 328.29 Å was eliminated after the subtraction as was that due to the intrinsic Fe XVI 335.4 Å.

The photometric calibration of the spectrograph was obtained by using the synchrotron radiation of Synchrotron Ultraviolet Radiation Facility (SURF II) (Ref. 29) at

TABLE I. The electron temperature and density at emission peaks. PL is the peak location to the plasma center, T_e is the measured electron temperature, IET is the calculated ionization equilibrium temperature, HIP is the half ionization potential.

Ions	Cl XIV	Ar XV	K XVI	Ca XVII	Sc XVIII	Ti XIX	V XX	Cr XXI
PL (cm)	19		16	14	10	8	8	<6
n_e (10^{13} cm^{-3})	1.5		2.5	3.1	3.9	4.3	4.3	5.3
T_e (eV)	210		370	420	650	720	720	>800
IET (eV)	294[a]	354[a]	432[b]	546[b]		700[a]		840[a]
HIP[c] (eV)	375	428	483	543	605	671	743	817

[a]Reference 24.
[b]Reference 25.
[c]Reference 26.

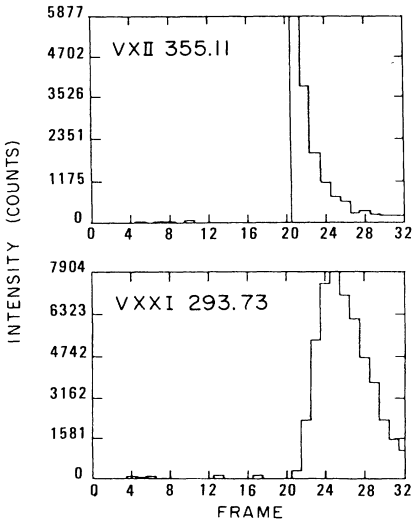

FIG. 4. Example of time history plots for vanadium ion lines as indicators of ionization stages. The GRITS started taking spectra at 144.33 ms. The laser fired at 250 ms. The spectral integration time is 5.424 ms. The vanadium lines appeared after frame 20. With increasing ionization stage, the lines rise more slowly after the injection and remain in the plasma for a longer time.

the National Bureau of Standards. The uncertainty of the photometric calibration was estimated by including various sources of error. These sources were due to the scattered synchrotron light, the contribution of higher-order grating diffraction, the precision of the alignment of the instrument with respect to the synchrotron, the nonuniform grating reflectivity, the uncertainty in the detector gain as a function of applied voltage, and the uncertainty in the calculation of the f number for each wavelength. Uncertainty of the absolute photometric calibration varies at different positions of the detector but it is less than 30%. The calibration for the pixels at the center region of the detector (pixel 250 to pixel 750) is more reliable than that at the edges. For a pair of lines, the uncertainty of the *relative* photometric calibration is generally smaller but varies significantly with the positions of the lines. For example, in the case of two close lines recorded near the center of the detector during the same shot, the uncertainty of the relative photometric calibration is less than 5%. For those lines appearing at the center region of the detector at two adjacent detector positions along the Rowland circle, the estimated uncertainty of the relative photometric calibration should be less than 20%. In our case, the lines studied were spread from ~ 150 to ~ 348 Å and some of them were located at pixels close to the detector edge regions. However, the uncertainty of the relative photometric calibration used for the data reported here is 25% or less.

In order to get better signal-to-noise ratios in the intensity measurements, a spectrum containing the peak line intensity following the injection and two consecutive frames following it were added together. Thus the effective integration time of the signals became 16.2 ms. The uncertainty of the measurements due to the imperfect removal of the noisy background depended on the intensity of the signal. For the resonance $2s^2\,{}^1S_0-2s2p\,{}^1P_1$ transition lines the uncertainties were negligible. But the uncertainties for other weaker lines measured could be as large as 20%.

Some of the features were partially blended, but the linear properties of the detector permitted separation of the features in many cases. For instance, the Ca XVII $2s^2\,{}^1S_0-2s2p\,{}^1P_1$ line at 192.85 Å was blended with another feature leading to a bump on its longer wavelength side. To separate this bump from the line studied, a Gaussian fit,

$$A_0+\sum_{n=1}^{3} A_n \exp[-(X-X_n)^2/\sigma_n^2]$$

with A_n, X_n, and σ_n adjustable, was applied. (A variable linewidth was used because the detector plane is mounted on the tangent of the Rowland circle and the slit image therefore changes its width along the plane.) Figure 5 shows the results of the fitting procedure. The long-wavelength feature is 1 Å above the Ca XVII 192.85-Å line. It is identified as Ca XIV 193.88 Å with an intensity of 1.7 relative to Ca XIV 186.61 Å (not shown). In addition there is a weak unidentified feature at 191.70 Å. The total intensity of these two small features was only $\frac{1}{9}$ relative to the Ca XVII 192.85-Å line.

The $2s^2\,{}^1S_0-2s2p\,{}^1P_1$ resonance transition lines (designated S) of Sc XVIII, Ti XIX, V XX, and Cr XXI were blended with a weak N I–like ion line belonging to the $2s^22p^3\,{}^4S_{3/2}-2s2p^4\,{}^4P_{5/2}$ transition (N).[30] However, there was another unblended N I–like ion line of the $2s^22p^3\,{}^4S_{3/2}-2s2p^4\,{}^4P_{3/2}$ transition (N^*) in the vicinity of each S line, which could be measured. According to Refs. 32, 32, and 16, the N/N^* line ratio is about 1.5 for all elements considered in the range of our electron densities. In the cases of Ar, K, and Ca, where these lines are separable, the N I–like line ratios were found to have

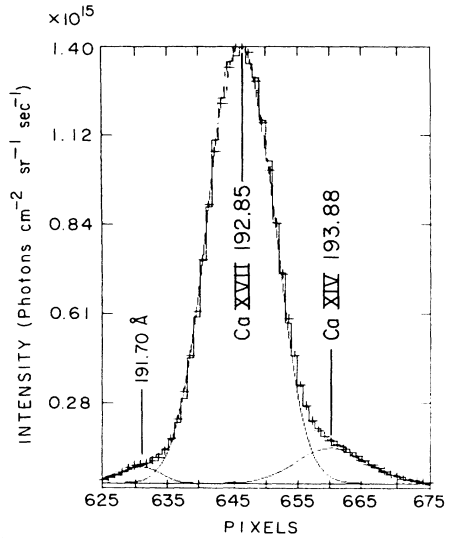

FIG. 5. Separation of blended Ca XVII 192.85 Å and Ca XIV 193.88 Å, and an unidentified feature at 191.70 Å. See the text for the fitting technique.

similar values. Thus the N line brightness could be estimated and subtracted from the total brightness of the blended S and N lines. In case of Cl XIV, the S line was blended with the N^* line. Then the N line was measured and the N^* line brightness was estimated to obtain the correct S line brightness. Note that the contribution of the N I—like ion lines to the singlet Be I—like transitions did not exceed 8% for Cl XIV, Sc XVIII, Ti XIX, and V XX, and it was less than 16% for Cr XXI.

Another possible source of error is that the plasma conditions might have changed from shot to shot when data from different shots were compared. However, the injection reproducibility was confirmed by monitoring brightnesses of different lines emitted by the same injected element during different shots. For instance, during scandium injection a normal incidence time-resolving spectrometer[33] at the same toroidal location measured the brightnesses of the Sc X line at a wavelength of 422.9 Å. In this case, the brightnesses changed from shot to shot by 5% or less. The data sets discussed here were taken from those shots in which the monitor line brightness changed by less than 10%.

All together, the estimated cumulative uncertainty of the measured relative brightnesses was less than 34%.

III. DISCUSSION OF THE RESULTS

The Be I—like ion lines identified in this experiment are listed in Table II, along with Edlén's calculated wavelengths[9] which are expected to be accurate to 0.01 Å. The intercombination lines of the $2s^2\,{}^1S_0$—$2s2p\,{}^3P_1$ transition were identified for the first time for Sc XVIII and V XX, and measured for the first time in a tokamak plasma for Ar XV and Cr XXI. The $2s^2\,{}^1S_0$—$2s2p\,{}^1P_1$ line of V XX at 159.35 Å was also newly identified. All the lines of the $2s2p\,{}^3P$—$2p^2\,{}^3P$ transitions listed were measured in a tokamak plasma for the first time. Within the wavelength calibration accuracy of ±0.2 Å for the spectrograph, there are no apparent discrepancies between the measured and the calculated wavelengths.

The primary interest of this study, however, is in the line intensity ratios. As mentioned at the beginning of this paper, the distorted-wave approximations used in the computation of electron collision strengths are inadequate for the low-Z Be I—like ions because of neglect of the resonance structure and the channel-coupling effects. The experimental results[17] for C III to Ne VII agreed very well with the theoretical calculations with the R-matrix method which included these effects, but not with those based on the distorted-wave approximation. However, Table III, which compares these two types of computations[10,11,18,19] for Ca XVII at the tokamak plasma conditions, shows good agreement between the two theoretical approaches. It indicates that the predictions of the two approaches may converge for moderately-high-Z elements.

Although the two calculations each used a different number of levels, the resulting effect is expected to be small. The distorted-wave calculation[10,18] included 20 levels of the $2s^2$, $2s2p$, $2p^2$, and $2s3l$ configurations in the model, while the R-matrix calculation[11,19] used a ten-level model of the $2s^2$, $2s2p$, and $2p^2$ configurations. The effects of mixing the $n=3$ configurations in the target wave functions in the electron-impact transition strengths within $n=2$ are, in general, small.[10] (An exceptional case here is the $2s^2\,{}^1S_0 \rightarrow 2p^2\,{}^1D_2$ transition strength which was changed by 25%, but the transition strength is so small that this does not affect the line ratios R and R^* defined in Sec. I.) The cascades from the $n=3$ levels in the model should cause changes of only a few percent in the line-intensity ratios computed for tokamak plasma conditions. Therefore, including the $2s3l$ levels in the model changes the predicted line ratios by values much less than the uncertainty in the experimental measurements.

The importance of the electron interaction terms which

TABLE II. The identified Be I—like lines (Å). c in the first column represents wavelength calculated by Edlén (Ref. 9) and m the measured values.

Transitions	Cl XIV	Ar XV	K XVI	Ca XVII	Sc XVIII	Ti XIX	V XX	Cr XXI
				$2s2s$-$2s2p$				
$c\ {}^1S_0$-${}^1P_1$	237.81	221.13	206.25	192.85	180.69	169.58	159.35	149.89
$m\ {}^1S_0$-${}^1P_1$	237.8	221.1	206.3	192.9	180.7	169.6	159.4	149.9
$c\ {}^1S_0$-${}^3P_1$	455.53	423.98	396.01	371.05	348.61	328.34	309.94	293.16
$m\ {}^1S_0$-${}^3P_1$		423.4[a]			348.4	328.3	309.9	293.2
				$2s2p$-$2p2p$				
$c\ {}^3P_2$-${}^3P_2$	286.22	266.24	248.56	232.81	218.73	206.09	194.71	184.45
$m\ {}^3P_2$-${}^3P_2$	286.3	266.3	248.5	232.9	218.9	206.0	194.6	184.5
$c\ {}^3P_0$-${}^3P_1$	279.75	258.77	253.67	223.02	207.60	193.51	180.56	168.60
$m\ {}^3P_0$-${}^3P_1$					207.7		180.6	168.6
$c\ {}^3P_1$-${}^3P_1$	284.31	263.67	245.30	228.73	213.69	199.88	187.17	175.42
$m\ {}^3P_1$-${}^3P_1$				228.8	213.6			
$c\ {}^3P_2$-${}^3P_1$	295.02	275.91	259.05	244.04	230.60	218.52	207.56	197.54
$m\ {}^3P_2$-${}^3P_1$		276.3						
$c\ {}^3P_1$-${}^3P_2$	276.04	254.83	235.88	218.84	203.43	189.44	176.69	165.01
$m\ {}^3P_1$-${}^3P_2$	276.1	254.9			203.4			

[a]Measured by the normal incidence time-resolving spectrograph.

TABLE III. Comparison of computed relative emissivities for Ca XVII. At $n_e = 1\times10^{13}$ cm^{-3} and $T_e = 6.3\times10^6$ K, $d = (B-D)/[(B+D)/2]$, where d is the discrepancy, B represents the distorted-wave value, and D represents the R-matrix value.

λ (Å)	Transitions	Distorted-wave[a]	R-matrix[b]	Discrepancy (%)
370.81	$2s2s\ ^1S_0-2s2p\ ^3P_1$	3.19	3.04	+ 4.8
193.06	$2s2s\ ^1S_0-2s2p\ ^1P_1$	100.	100.	0.0
238.67	$2s2p\ ^3P_1-2p2p\ ^3P_0$	1.83×10^{-2}	2.14×10^{-2}	−15.6
585.83	$2s2p\ ^1P_1-2p2p\ ^3P_0$	1.33×10^{-5}	1.81×10^{-5}	−30.6
233.04	$2s2p\ ^3P_0-2p2p\ ^3P_1$	6.99×10^{-1}	4.93×10^{-1}	+ 34.6
228.93	$2s2p\ ^3P_1-2p2p\ ^3P_1$	4.80×10^{-1}	3.41×10^{-1}	+ 33.9
244.07	$2s2p\ ^3P_2-2p2p\ ^3P_1$	6.58×10^{-1}	4.72×10^{-1}	+ 32.9
530.44	$2s2p\ ^1P_1-2p2p\ ^3P_1$	1.73×10^{-4}	1.40×10^{-4}	+ 21.1
219.17	$2s2p\ ^3P_1-2p2p\ ^3P_2$	7.60×10^{-1}	5.71×10^{-1}	+ 28.4
233.01	$2s2p\ ^3P_2-2p2p\ ^3P_2$	1.81	1.33	+ 30.6
480.85	$2s2p\ ^1P_1-2p2p\ ^3P_2$	1.07×10^{-2}	1.01×10^{-2}	+ 05.7
189.40	$2s2p\ ^3P_1-2p2p\ ^1D_2$	9.34×10^{-3}	8.96×10^{-3}	+ 02.1
199.65	$2s2p\ ^3P_2-2p2p\ ^1D_2$	1.14×10^{-1}	1.05×10^{-1}	+ 08.2
357.55	$2s2p\ ^1P_1-2p2p\ ^1D_2$	3.70×10^{-1}	3.22×10^{-1}	+ 13.9
143.54	$2s2p\ ^3P_1-2p2p\ ^1S_0$	3.10×10^{-4}	4.31×10^{-4}	−32.7
223.04	$2s2p\ ^1P_1-2p2p\ ^1S_0$	1.65×10^{-1}	1.94×10^{-1}	−16.8

[a]Bhatia *et al.* (Ref. 18).
[b]Dufton *et al.* (Refs. 11 and 19).

produce the coupling between channels decreases with both increasing electron-impact energy and increasing ionic charge.[34] In addition, the resonance structure is important only if the energy of the impacting electron is close to the threshold energy of the transition concerned.[35] Thus one can expect the collision strengths based on the distorted-wave approximation to be accurate at high ionic charges and high impact energies. In the case of Be I–like ions of Cl to Cr, the ionic charges are moderately high, and ionization potentials are an order of magnitude higher than the transition energies. The ions studied here exist in a high-electron-temperature plasma. At this high electron temperature only a very small portion of electrons have energies near the transition threshold energy. Since the effective collision strength is a statistical average over the electron energy, the effects of the channel coupling and the resonance structure in the calculated line intensity ratios should be small enough to be neglected as they are in the distorted-wave approximation.

The minor discrepancies between the results of the two types of computations for Ca XVII presented in Table III probably can be attributed to an accumulation of all of the above small differences. However, even though the predictions of the two theoretical techniques appear to agree, this does not guarantee that they are correct and it is extremely important to compare these predictions with experimental measurements.

The line-intensity ratios, R and R^*, for the elements in this study are insensitive to either the electron temperature or the electron density in the range of the tokamak plasma conditions. Test calculations were made for Ar XV, Ca XVII, and Ge XXIX at different plasma conditions. After increasing the temperature from the half ionization potential by 50%, the line ratios R and R^* increased by only 10% for Ar, by 15% for Ca XVII, and by 10% for Ge XXIX.[36] Therefore, the electron-temperature dependence of these line-intensity ratios is not expected to be noticeable within the existing experimental accuracy.

The line-ratio computations also showed little electron-density dependence of R and R^* in the tokamak electron-density range.[10,11,18,19] The experimental and theoretical values of R and R^* for Sc XVII and Ti XIX at various electron densities are presented in Fig. 6. In no case is there evidence for a strong electron-density dependence.

The measured and computed line ratios for Cl XIV to Cr XXI at an average line electron density near 3.5×10^{13} cm^{-3} are listed in Table IV and presented as a function of Z in Fig. 7. The calculated line ratios were taken from Bhatia *et al.*[18] for Ar XV, Ca XVII Ti XIX, and Cr XXI and were extrapolated or interpolated for the other

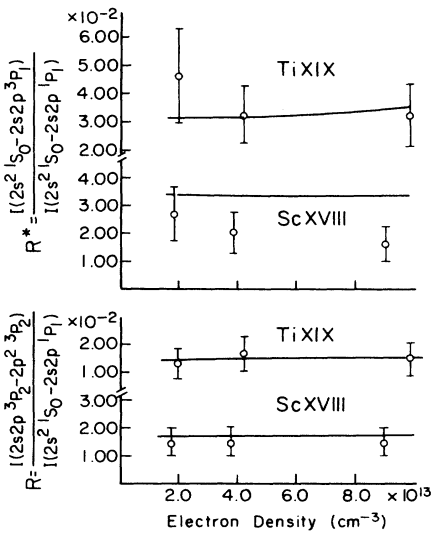

FIG. 6. The experimental density dependences of the line ratios of Sc XVIII and Ti XIX compared with the theoretical predictions of Bhatia *et al.* (Ref. 18) (solid line). The electron densities are taken at the peak of the volume emission shell.

TABLE IV. The relative intensities of Be I–like ion lines at $\langle n_e \rangle = 3.5 \times 10^{13}$ cm^{-3}. R and R^* are defined in Eq. (1) and Eq. (2). In the first column m represents measured, c represents calculated by Bhatia *et al.* (Ref. 18), and interpolated between electron densities. S_m is the measured line intensity of the $2s^2\,{}^1S_0$-$2s2p\,{}^1P_1$ transition.

	Cl XIV	Ar XV	K XVI	Ca XVII	Sc XVIII	Ti XIX	V XX	Cr XXI	Average
$10^{-2}R^*$									
m					2.05	3.12	2.87	3.53	
c	3.21[a]	3.26	3.39[b]	3.57	3.33[b]	3.11	3.49[b]	3.81	
R_m^*/R_c^*					0.62	1.00	0.82	0.93	0.84±0.17
$10^{-2}R$									
m	3.70		2.51	1.66	1.54	1.76	1.17	0.92	
c	2.78[a]	2.53	2.28[b]	2.02	1.77[b]	1.52	1.28[b]	1.05	
R_m/R_c	1.33		1.10	0.82	0.87	1.16	0.91	0.88	1.01±0.19
Measured absolute line brightness in 10^{14} (photons/sterad cm^2 sec)									
S_m	87.0	s[c]	116.0	197.0	360.0	309.0	317.0	156.0	

[a]Extrapolated along Z.
[b]Interpolated along Z.
[c]Saturated.

elements. In the computation of Bhatia *et al.*, the electron temperature was set at half of the ionization potential for each ion, and electron densities were set at 3.5×10^{13} cm^{-3}. Figure 7 shows that the measured R line-ratio points are scattered around a straight line connecting the points predicted by distorted-wave calculations. The calculated R^* ratios were scattered about a horizontal line at 3.4×10^{-2}. The agreement between experiment and theory is quite good except for the case of R^* for Sc XVIII. Table IV lists the ratios of measured to calculated values, R_m/R_c and R_m^*/R_c^*. The two arithmetic means for the ratios of the experimental to calculated values are 1.01±0.19 and 0.84±0.17, respectively. Thus it appears that the agreement between experimental and theory is quite good, well within the experimental uncertainties discussed in Sec. II.

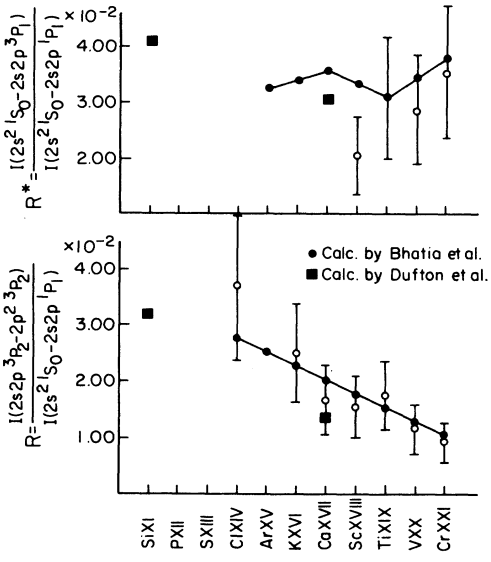

FIG. 7. Comparison of the measured line ratios, R and R^*, at the average electron density of 3.5×10^{13} cm^{-3} with calculations of Bhatia *et al.* (Ref. 18) based on the distorted-wave approximation and Dufton *et al.* (Refs. 11 and 19) based on the R-matrix method.

The R-matrix-method calculations of Dufton *et al.* are available only for two cases in this range, Si XI (Ref. 37) and Ca XVII. The values are close to the distorted-wave-approximation results for Ca XVII and to an extrapolation of the distorted-wave values for Si XI. A direct comparison with experimental data is available only in the case of Ca XVII for which the R line ratio was measured and is within 25% of both theoretical calculations.

In a previous paragraph Fig. 6 was used to show that the variations of R and R^* with electron density are negligible as expected on the basis of the theoretical calculations. One can also use the data of Fig. 6 in an inverse argument. An electron-density dependence is not expected on theoretical grounds, unless the theoretical calculations are very far off the mark. Figure 7 and Table IV indicate they are not. Then, the changes in the measured values of R and R^* for quite different discharge conditions, caused by changing the electron density over a range of about a factor of 5, indicate the magnitude of the experimental errors associated with noise, shot-to-shot variations in the emission brightnesses, and changes in the character of the spectra with changes in the plasma conditions. Table V lists the electron-density dependence of the brightness of the R and R^* ratios at these line average electron densities. The percentage standard deviation listed for the measured values of R and R^* are consistent with the experimental uncertainties discussed in Sec. II.

Which relative collision strengths has this experiment checked and to what extent are the results of these experiments valid at other, particularly lower, densities? The effect of uncertainties in the computed collision strengths, $\delta\Omega_{ij}$, on uncertainties in the computed line intensity ratio, δR, can be expressed by

TABLE V. The variation of Be I–like ion line intensity ratios R and R^* for discharges of different electron density. m indicates measured values, x represents no measurements, and c indicates values calculated by Bhatia, *et al.* (Ref. 18), and interpolated along the electron density.

$\langle Ne \rangle$ (10^{13} cm^3)		1.6		3.5		8.0			
Ratios	Ions	m	c	m	c	m	c	Average m/c	σ%
$10^{-2}R^*$	Ca XVII	x	3.56	x	3.57	x	3.56		
	Sc XVIII	2.73	3.46[a]	2.05	3.33[a]	1.57	3.40[a]	0.62±0.16	26%
	Ti XIX	4.66	3.11	3.12	3.11	3.26	3.50	1.14±0.31	27%
$10^{-2}R$	Ca XVII	x	1.99	1.66	2.02	x	2.07		
	Sc XVIII	1.53	1.72[a]	1.54	1.77[a]	1.54	1.80[a]	0.88±0.02	2%
	Ti XIX	1.34	1.42	1.76	1.52	1.53	1.54	1.03±0.11	11%
Measured absolute brightness of $2s^2\,{}^1S_0$–$2s2p\,{}^1P_1$ lines in 10^{14} (photons/sr cm^2 sec)									
	Sc XVIII	78		360		177			
	Ti XIX	54		309		107			

[a]Interpolated along Z. σ is the standard deviation as percentage.

$$\delta R = \sum_{i,j} (\partial R/\partial \Omega_{ij}) \delta \Omega_{ij} \ . \tag{3}$$

Since one is normally interested in the percentage change in R for a percentage change in Ω_{ij}, the sensitivity of the ratio R to a given collision strength is best expressed by

$$S = \text{abs}[(\Omega_{ij}/R)(\partial R/\partial \Omega_{ij})] \ . \tag{4}$$

A similar pair of equations hold for R^*. The quantity S was estimated for Ca XVII using the collision strengths of Bhatia *et al.*[10] For R^*, the values of S are about 1.0, 0.44, and 0.40 for the $2s^2\,{}^1S_0$–$2s2p\,{}^1P_1$, $2s^2\,{}^1S_0$–$2s2p\,{}^3P_1$, and $2s^2\,{}^1S_0$–$2s2p\,{}^3P_2$ transitions, almost independent of density. Other collision strengths contribute in negligible amounts. For R, the density-dependent ratio, the situation is slightly more complex. Figure 8 shows the dependence of the most important sensitivities as a function of electron density. At a density of 3×10^{13} cm^{-3}, where the tokamak measurements were made, the $2s^2\,{}^1S_0$–$2s2p\,{}^3P_2$, $2s2p\,{}^3P_2$–$2p^2\,{}^3P_2$, and $2s2p\,{}^3P_2$–$2p^2\,{}^3P_1$ transitions dominate followed by the $2s^2\,{}^1S_0$–$2s2p\,{}^1P_1$ transition. These transitions are important down to densities of about 3×10^{10} cm^{-3} where the $2s^2\,{}^1S_0$–$2p^2\,{}^3P_2$ becomes significant. The tokamak data provide no data on this collision strength, which involves a spin change and the promotion of two electrons from $2s^2$ to $2p^2$. Note, however, that at densities below 3×10^{10} cm^{-3}, the value of R is near 10^{-3} and accurate spectroscopic measurements become more difficult. Thus it appears that the tokamak experiments have checked the collision strengths for the most important transitions and it is likely that theoretical values of R will be accurate in the electron-density range from 10^{14} down to 10^{11} cm^{-3} for Ca XVII. For other ions the lower limit will shift with Z.

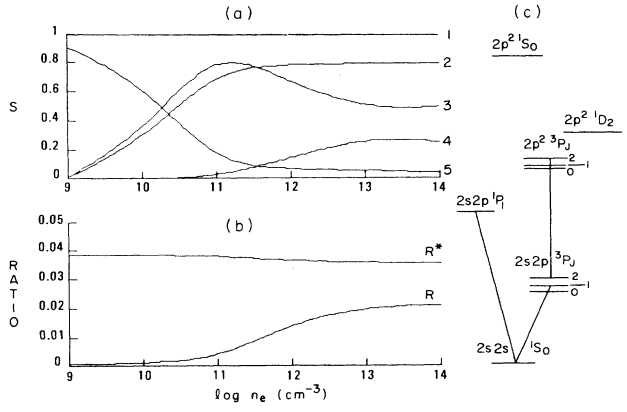

FIG. 8. (a) S, defined in Eq. (4), indicates the sensitivity of the value of R to uncertainties in the collision strengths and the dominant collision strengths controlling the level populations which determine R. The values of the most important transitions for the line brightness ratio R for Ca XVII are plotted as functions of electron density. The numbered curves with respect to the electron collisional transitions are (1) $2s^2\,{}^1S_0$–$2s2p\,{}^1P_1$, (2) $2s^2\,{}^1S_0$–$2s2p\,{}^3P_2$, (3) $2s2p\,{}^3P_2$–$2p^2\,{}^3P_2$, (4) $2s2p\,{}^3P_2$–$2p^2\,{}^3P_1$, and (5) $2s^2\,{}^1S_0$–$2p^2\,{}^3P_2$. (b) The emissivity ratios R and R^* defined in Eqs. (1) and (2) are plotted as function of electron density for Ca XVII, Bhatia *et al.* (Ref. 18). (c) The grotrian diagram of $n=2$ levels of Ca XVII.

IV. CONCLUSION

For the Be I–like ions, Cl XIV to Cr XXI, at electron temperatures near the ionization equilibrium and electron densities of $\sim10^{13}$ to 10^{14} cm^{-3}, the experimentally determined line ratios R and R^* agree with theoretical calculations by Bhatia *et al.*,[18] which are based on the distorted-wave approximation. The ratios of the measured to calculated values of R and R^* were 1.01±0.19 and 0.84±0.17, respectively. For the one case where an R-matrix-method value was available, Ca XVII, good agreement also exists. One exception to this general agreement between experiment and theory is the value of R^* for Sc XVIII; this case clearly needs additional investigation, both theoretical and experimental. There is no evidence for a dependence of R and R^* on the electron density in this range in agreement with the theoretical calculations.

The theoretical collision strengths which dominate the calculated level populations and hence the line ratios have been verified by this laboratory study. For Ca XVII, these

collision strengths were identified and the same collision strengths are important over the electron-density range $10^{11}-10^{14}$ cm^{-3}, implying that the theoretical predictions of level populations for Ca XVII are expected to be accurate over that range. For other ions, the lower density limit will shift with Z. The agreement of the distorted-wave-approximation computation with the experimental results serve as evidence that the resonance structure and channel-coupling effects are not important in the computation of average electron-ion collision excitation rates for the Be I—like ions at moderately high Z. This agreement also gives assurance that the theoretical calculations can be relied on for plasma diagnostics.

Finally, we note that the value of R in Ca XVII for the August 9, 1973 solar flare discussed in Sec. I is still inconsistent. The experimental determination of this ratio reported here is within 25% of the theoretical calculations. Thus it would seem that the measured solar flare ratio is either inaccurate or due to some complication in the flare that cannot be described by a simple model.

ACKNOWLEDGMENTS

The authors are grateful to D. L. Dufton for making his calculation of Ca XVII at higher electron density available. We wish to thank the entire TEXT group for the excellent collaboration during the experiment. This work is sponsored by the Department of Energy under Grant No. DE-FG02-85ER53214 to The Johns Hopkins University and Contract No. DE-AC05-78ET53043 to the University of Texas.

*Permanent address: Princeton Plasma Physics Laboratory, Princeton University, Princeton, NJ.

[1]B. C. Fawcett, A. Ridgely, and A. T. Hatter, J. Opt. Soc. Am. **70**, 1349 (1980).

[2]K. D. Lawson and N. J. Peacock, J. Phys. B **13**, 3313 (1980).

[3]J. C. Purcell and K. G. Widing, Astrophys. J. **176**, 239 (1972).

[4]K. P. Dere, H. E. Mason, and A. K. Bhatia, Astrophys. J. Suppl. Ser. **40**, 341 (1979).

[5]M. F. Stamp and N. J. Peacock, J. Phys. B **15**, L703 (1982).

[6]E. Hinnov, S. Suckewer, S. Cohen, and K. Sato, Phys. Rev. A **25**, 2293 (1982).

[7]TFR Group, Phys. Lett. **74A**, 57 (1979).

[8]E. Hinnov, Astrophys. J. Lett. **230**, L197 (1979).

[9]B. Edlén, Phys. Scr. **28**, 51 (1983).

[10]A. K. Bhatia and H. E. Mason, Astron. Astrophys. Suppl. Ser. **52**, 115 (1983).

[11]P. L. Dufton, A. E. Kingston, J. G. Doyle, and K. G. Widing, Mon. Not. R. Astron. Soc. **205**, 81 (1983).

[12]H. Nussbaumer and P. J. Storey, J. Phys. B **12**, 1647 (1979).

[13]S. Suckewer, Phys. Scr. **23**, 72 (1981).

[14]I. Yu. Skobelev and S. Ya. Khahkalin, Opt. Spectrosc. (USSR) **54**, 13 (1983).

[15]L. A. Vainshtein, I. I. Sobelman, and E. A. Yukov, *Excitation Cross Section of Atoms and Ions by Electrons* (Nauka, Moscow, 1973).

[16]B. C. Stratton, H. W. Moos, S. Suckewer, U. Feldman, J. F. Seely, and A. K. Bhatia, Phys. Rev. A **31**, 2534 (1985).

[17]M. Finkenthal, T. L. Yu, S. Lippmann, L. K. Huang, B. Stratton, H. W. Moos, W. Hodge, and A. K. Bhatia, Astrophys. J. (to be published).

[18]A. K. Bhatia, U. Feldman, and J. F. Seely, At. Data Nucl. Data Tables (to be published).

[19]P. L. Dufton, A. E. Kingston, and N. S. Scott, J. Phys. B **16**, 3053 (1983).

[20]K. W. Gentle, Nucl. Technol./Fusion **1**, 479 (1981).

[21]E. Marmar, J. Cecchi, and S. Cohen, Rev. Sci. Instrum. **46**, 1149 (1975).

[22]W. L. Hodge and H. W. Moos, Rev. Sci. Instrum. **55**, 16 (1984).

[23]H. R. Griem, *Plasma Spectroscopy* (McGraw-Hill, New York, 1964), p. 176.

[24]C. Breton, C. DeMichelis, M. Finkenthal, and M. Mattioli, Association Euratom-CEA, Fontenay-aux-Roses, Report No. EUR-CEA-FC-948, (1978) (unpublished).

[25]M. Landini and B. C. Monsignori Fossi, Astron. Astrophys. Suppl. Ser. **7**, 291 (1972).

[26]S. Bashkin and J. Stoner, *Atomic Energy Levels and Grotrian Diagrams* (North-Holland, Amsterdam, 1981).

[27]M. Finkenthal, R. Bell, and H. W. Moos, Phys. Lett. **88A**, 165 (1982).

[28]M. Finkenthal, R. Bell, and H. W. Moos, J. Appl. Phys. **56**, 2012 (1984).

[29]D. L. Ederer, E. B. Saloman, S. C. Ebner, and R. P. Madden, J. Res. Nat. Bur. Stand., Sect. A **79**, 791 (1975).

[30]B. Eldén, Phys. Scr. **30**, 135 (1984).

[31]U. Feldman, G. A. Doschek, C. C. Cheng, and A. K. Bhatia, J. Appl. Phys. **51**, 190 (1980).

[32]A. K. Bhatia, U. Feldman, and G. A. Doschek, J. Appl. Phys. **51**, 1464 (1980).

[33]R. E. Bell, M. Finkenthal, and H. W. Moos, Rev. Sci. Instrum. **52**, 1806 (1981).

[34]J. Callaway, Adv. Phys. **29**, 771 (1980).

[35]K. A. Berrington, J. Phys. B **18**, L395 (1985).

[36]A. K. Bhatia (private communication).

[37]F. P. Keenan, K. A. Berrington, P. G. Burke, and A. E. Kingston, Mon. Not. R. Astron. Soc. **207**, 459 (1984).